Spring 2013

CFD simulation of void flow in ECCS

Lifeng Wang

Department: Mining and Nuclear Engineering

CFD SIMULATION OF VOID FLOW

IN ECCS

by

LIFENG WANG

A THESIS

Presented to the Faculty of the Graduate School of the

MISSOURI UNIVERSITY OF SCIENCE AND TECHNOLOGY

In Partial Fulfillment of the Requirements for the Degree

MASTER OF SCIENCE IN NUCLEAR ENGINEERING

2013

Approved by:

Ayodeji B. Alajo, Advisor

Shoaib Usman

Gary E. Mueller

ABSTRACT

Emergency core cooling system (ECCS) has been studied extensively for reactor safety. Emergency core cooling system (ECCS) is designed to make sure the reactor core it is protected by providing sufficient heat removal during accident conditions. In a loss-of-coolant-accident (LOCA) scenario, the ECCS is designed to take over the reactor core cooling by drawing water from a reservoir or tank. Voids may be introduced into the ECCS through a variety of means leading to total or partial loss of suction supply, or through gas depressurization resulting from difference in gas saturation pressure and ambient pressure. The transportation of voids through the ECCS train may lead to malfunction and/or degeneration of the ECCS – a safety concern. The issues associated with void introduction in ECCS include but are not limited to pipe damage, suction pump failure and stress-induced failures.

In this thesis, simulations were performed to determine the maximum void allowable at a gas accumulation point in the ECCS piping system. The limiting criterion was set at 5% maximum void fraction at the inlet to the any of the ECCS pumps. The simulation was performed using FLUENT 6.3 – a computational fluid dynamics (CFD) code. The maximum void allowable in the ECCS pump was determined for 2 ECCS models. The allowable void at the accumulation point in each models are 2.1447 ft^3 for Model 1 and 1.1503 ft^3 for Model 2. The times at which the maximum void fractions were reached at the pump entry are 28 and 22 seconds for Models 1 and 2, respectively.

ACKNOWLEDGMENTS

The author thanks Sipaun, Susan M. and Yigit, Cemil for their assistance during simulation. The author greatly appreciates the thoughtful and constructive suggestions from her academic advisor, Dr. Alajo, Ayodeji Babatunde; the research was significantly improved because of his input. The author also appreciates the assistance provided by her committee members, Dr. Gary E. Mueller and Dr. Shoaib Usman.

TABLE OF CONTENTS

Page

LIST OF ILLUSTRATIONS

Page

LIST OF TABLES

Page

1. INTRODUCTION

The emergency core cooling system (ECCS) is an important part of the design element for the loss of coolant accident (LOCA). In the event of a LOCA, the ECCS is designed to provide decay heat removal to a reactor core as provided in chapter 50.46 in Title 10 of the U.S. code of federal regulations (10 CFR 50.46). The U.S. nuclear regulatory commission (NRC) set fifth the following requirements for the ECCS to meet its regulatory compliance:

- Peak cladding temperature must not exceed 2200^0F (~1200^0C).
- Maximum cladding oxidation must not exceed 17% of the pre-oxidation total cladding thickness.
- Maximum hydrogen generation must not exceed 1% of the hypothetical amount that would be generated if all cladding metal surrounding the active fuel were oxidized.
- Coolable geometry must be maintained.
- Long-term cooling must be maintained to remove decay heat for the necessary length of time.

The five requirements summarized above provide a framework for evaluating the cooling performance of any ECCS. [2] As part of such evaluations, it is also important to know the conditions under which any or all of the requirements would be compromised. One of such conditions is the introduction of void into the ECCS. In a LOCA scenario, the ECCS is designed to take over the reactor core cooling by drawing water form a reservoir of tank. Voids may be introduced into the ECCS through a variety of means leading to total or partial loss of suction supply, or through gas depressurization resulting

from difference in gas saturation pressure and ambient pressure. The transportation of voids through the ECCS train may lead to malfunction and/or degeneration of the ECCS-a safety concern. In this thesis, the impact of void introduction into the ECCS is analyzed.

The objective of this study is to determine the maximum void allowable in emergency core cooling system (ECCS) and related equipment/systems in order to ensure proper function of the ECCS as designed. The analysis support this work was focused on the determination of the maximum void that would enter the ECCS pump upon the intrusion of gas into the ECCS piping. Voids intrusion into the suction of ECCS pumps could lead to pump binding and total or momentary loss of hydraulic performance, for example, mechanical damage, elevated pump vibration, catastrophic pump failure, and low suction pump trips. These events may result in pump shaft damage which could result in partial or total failure of the ECCS. In this work, criteria to justify operability of pumps under the intrusion of non-condensable gases were determined. This was achieved by developing models of typical ECCS piping and then analyzing the system using computational fluid dynamics code.

In recent years, computational fluid dynamics (CFD) technique has been used for a powerful tool to simulate and analyze behavior of the gas-liquid two-phase flow. Basing on the understanding of the physics driving the flow regime, appropriate models could be invoked to analyze all of the plausible phenomena in two-phase flow. One of the popular and robust CFD codes commercially available is FLUENT. In this work, FLUENT 6.3 was used to simulate the two-phase flow in two different ECCS piping systems. The gas behavior and variables that affect the two-phase flow will be discussed.

2. LITERATURE REVIEW

2.1. ECCS SYSTEM

Emergency core cooling system (ECCS) is designed to make sure the reactor core it is protected by providing sufficient heat removal during accident conditions. Under normal conditions, heat removal is achieved in the core via coolant circulation. In this case, the point at which heat transported from the core is dumped by the coolant depends on the reactor type. However, in accident conditions, the ECCS floods the core with water and is required to keep the core covered throughout the period needed to recover from the accident sequence. It is important to note that the ECCS allows a reactor plant to respond to a variety of accident-like loss of flow accident or loss of coolant accident (LOCA), to keep the maximum core temperature below the clad melting point. Thus, the issue of making sure the ECCS works as designed becomes a crucial matter.

Key components of the ECCS are the pumps used to transport water into the reactor core. These pumps are designed to transport single-phase water. Thus, an introduction of two-phase fluid into the pumps may compromise the ECCS. [1, 3]

2.2. BUBBLY TWO-PHASE FLOW

Bubbly two-phase flow is a mixed gas and liquid flow. The flow pattern is characterized by the presence of bubbles dispersed in a continuous liquid phase. Bubbly two-phase flow is a branch of fluid dynamics which studies a complex mixture of gas and fluid two-phase flow movement. This fluid flow type happens in many engineering fields and also could be found widely in nature. It is of great importance not only in various

kinds of industrial processes such as the power industry, chemical industry, energy, environment and metallurgy, but also in other technical field such as the space rocket propulsion, nuclear reactor heat removal. The study of two-phase flow developed rapidly in the 60s, and gradually became a new subject branch of fluid dynamics in the 80s to 90s.

The two-phase flow or multiphase flow is much more complicated than a single-phase flow. Two-phase flows are generally solved using correlations developed from practical engineering experience as well as experiments purposefully designed to develop valid empirical models. This places some limitations on the results obtained this way, since the validity of the results are limited to the conditions under which the empirical models were developed. In recent times, advancements in computational methods and computing power have improved the analysis of two-phase flow. The analysis of two-phase flow is readily done with computational fluid dynamics.[4-7]

2.3. COMPUTATIONAL FLUID DYNAMICS

2.3.1. Introduction. Computational fluid dynamics (CFD) is the analysis of fluid flow utilizing numeric methods in solving the flow problem. All CFD methods involve discretization of the flow system into tiny volumes, elements or streams. Thus a computer program is generally required to perform CFD analysis. The CFD programs are developed to analyze the fluid system-including fluid flow, heat transfer and other related physical phenomenon.

2.3.2. Computational Fluid Dynamics as a Research Tool. CFD can work harmoniously with experiment-not just providing a quantitative comparison, but also

providing a means to interpret a basic phenomenological aspect of the experimental conditions. [1] Due to the advancement in scientific and industrial sectors in which the physics of fluid flow is a key phenomenon, studies of fluid dynamics has become more and more important. In most cases, the cost of the experimental setup for a scaled complex fluid dynamic model is extremely expensive. CFD thus provide the avenue for reliable fluid flow analysis without the high cost associated with experimental setup. This makes CFD a widely accepted analysis tool for research in lieu of experiments. It is however important to note that CFD is also used in conjunction with experiments in verification and validation of CFD physics models and results.

2.3.3. The Governing Equations of Fluid. All of CFD are based on the fundamental governing equations of fluid dynamics-the continuity, momentum, and energy equations. The three fundamental physical principles upon which all of fluid dynamics are based on are:

- Mass conservation.
- Newton's second law, **F=ma**
- Energy conservation.

Not as a solid body, a fluid is in motion, so the velocity of each part of the body is different. For a continuum fluid, four models as showed in Figure 2.1 below are used to construct the fundamental physical principles for the fluid.

A. Finite control volume fixed in space with the fluid moving through it.
B. Finite control volume moving with the fluid such that the same fluid particles are always in the same control volume.
C. Infinitesimal fluid element fixed in space with the fluid moving through it.

D. Infinitesimal fluid element moving along a stream line with the velocity V equal to the local flow velocity at each point.

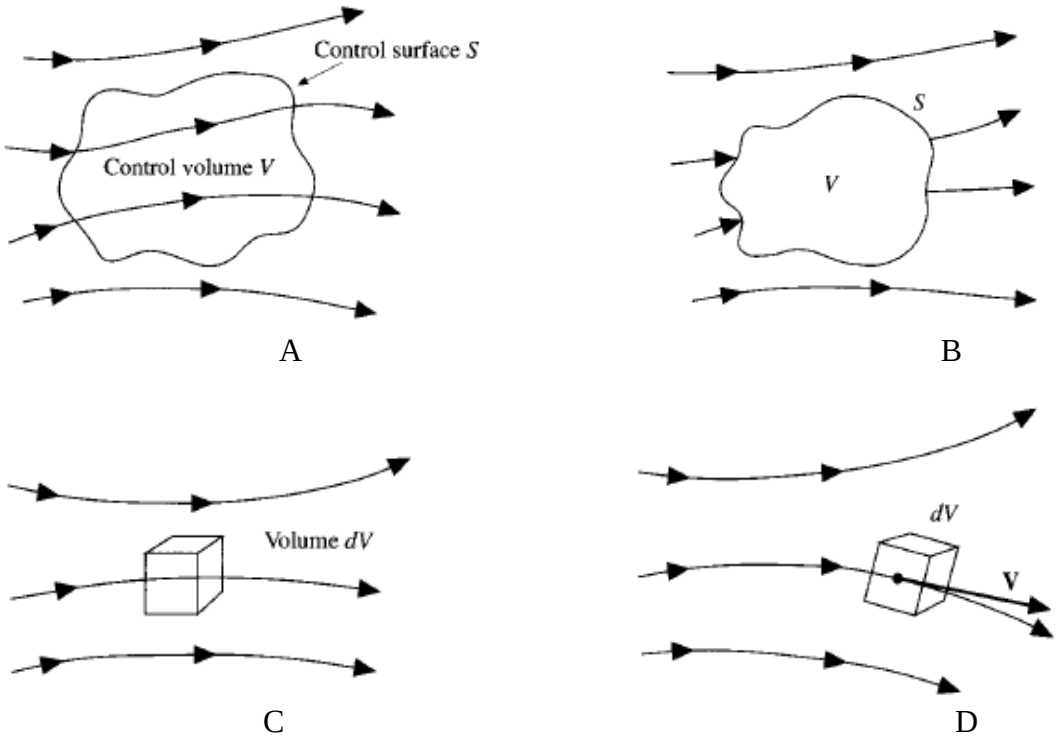

Figure 2.1: Four Fundamental Models Of A Continuum Fluid [8]

Control volume (V) is a closed volume drawn within a finite region of the flow and a control surface (S) is defined as the closed surface of volume boundary. Infinitesimal fluid element (dV) is an infinitesimally small fluid element in the flow with a differential volume dV. [7]

2.3.4. The Continuity Equation. Obtain an equation to represent the 1st fundamental physical principle : Mass is conserved, by applying this fundamental physical

principle into the finite control volume fixed in space with the fluid moving through model, finite control volume moving with the fluid and infinitesimal fluid element fixed in space model , then get the continuity equation.

$$\frac{\partial \rho}{\partial t} + \frac{\partial(\rho u)}{\partial x} + \frac{\partial(\rho v)}{\partial y} + \frac{\partial(\rho w)}{\partial z} = 0$$

Also, present as:

$$\frac{\partial \rho}{\partial t} + \nabla \cdot \left(\rho \vec{V}\right) = 0$$

When the fluid is uncompressible, ρ is a constant:

$$\nabla \cdot \vec{V} = 0$$

$\nabla \cdot \vec{V}$ is physically the time rate of change of the volume of a moving fluid element per unit volume.

For infinitesimally small fluid element moving with the flow, because of the fluid element has a fixed mass and its shape and volume will change as it moves downstream, so define the fixed mass and variable volume of this moving fluid element by δm and δv. Because the mass is conserved, the time rate of change of fluid element mass equal to 0 when the element moves along with the flow, then get:

$$\delta m = \rho \delta v$$

The continuity equation was presented as:

$$\frac{D\rho}{Dt} + \rho \nabla \cdot \vec{V} = 0$$

2.3.5. The Momentum Equation. Newton's second law, showed as the 2rd physical principle above, when applied to the moving fluid element with a vector relation which spited into three scalar relations along the x, y, and z axes, finds that the net force on the fluid element equals to the mass multiply by the acceleration of the element.

$F_x = ma_x$

$F_y = ma_y$

$F_z = ma_z$

Just considering the x component, there are two force sources for the left side: body forces and surface forces which present as:

Body force in x direction: $\rho f_x(dxdydz)$

Net surface force in x direction:

$$\left[p - (p + \frac{\partial p}{\partial x}dx\right]dydz + \left[\left(\tau_{xx} + \frac{\partial \tau_{xx}}{\partial x}dx\right) - \tau_{xx}\right]dydz + \left[\left(\tau_{yx} + \frac{\partial \tau_{yx}}{\partial y}dy\right) - \tau_{yx}\right]dxdz + \left[\left(\tau_{zx} + \frac{\partial \tau_{zx}}{\partial z}dz\right) - \tau_{zx}\right]dydx$$

The total force in the x direction F_x is a combination of above two forces, adding and cancelling terms, it is obtained:

$$F_x = \left[-\frac{\partial p}{\partial x} + \frac{\partial \tau_{xx}}{\partial x} + \frac{\partial \tau_{yx}}{\partial y} + \frac{\partial \tau_{zx}}{\partial z}\right]dxdydz + \rho f_x dxdydz$$

The mass of the fluid element is fixed:

$$m = \rho dxdydz$$

The component of acceleration in the x direction is:

$$\rho\frac{Du}{Dt} = -\frac{\partial p}{\partial x} + \frac{\partial \tau_{xx}}{\partial x} + \frac{\partial \tau_{yx}}{\partial y} + \frac{\partial \tau_{zx}}{\partial z} + \rho f_x$$

In a similar way, the y and z components can be obtained as:

$$\rho\frac{Dv}{Dt} = -\frac{\partial p}{\partial y} + \frac{\partial \tau_{xy}}{\partial x} + \frac{\partial \tau_{yy}}{\partial y} + \frac{\partial \tau_{zy}}{\partial z} + \rho f_y$$

$$\rho\frac{Dw}{Dt} = -\frac{\partial p}{\partial z} + \frac{\partial \tau_{xz}}{\partial x} + \frac{\partial \tau_{yz}}{\partial y} + \frac{\partial \tau_{zz}}{\partial z} + \rho f_z$$

2.3.6. The Standard $\mathbf{k-\varepsilon}$ Model. The determination of a turbulent length and time scale are solved by two separate transport equations using two-equation turbulence models. The standard $\mathbf{k-\varepsilon}$ model is a semi-empirical model based on model transport equations for the turbulence kinetic energy (k), and its dissipation rate (ε). It was proposed by B. E. Launder and D. B. Spalding, Lectures in Mathematical Models of Turbulence, Academic Press, London, England, 1972. [8] They build a mathematical model used for explaining the popularity in industrial flow and heat transfer simulations of a wide range of turbulent flow for robustness, economy, and reasonable accuracy. Because he derivation of the model equations relies on phenomenological considerations and empiricism, so it is a semi-empirical model.

In the derivation of the $k-\varepsilon$ model, the standard $k-\varepsilon$ model is only valid for fully turbulent flows, and the effects of molecular viscosity are negligible.

The turbulence kinetic energy (k) which derived from the exact equation and rate of dissipation (ε) which was obtained using physical reasoning and bears little resemblance to its mathematically exact counterpart, are obtained by the following transport equations:

$$\frac{\partial}{\partial t}(\rho k) + \frac{\partial}{\partial x_i}(\rho k u_i) = \frac{\partial}{\partial x_j}\left[\left(\mu + \frac{\mu_t}{\sigma_k}\right)\frac{\partial k}{\partial x_j}\right] + G_k + G_b - \rho\varepsilon - Y_M + S_k$$

$$\frac{\partial}{\partial t}(\rho\varepsilon) + \frac{\partial}{\partial x_i}(\rho\varepsilon u_i) = \frac{\partial}{\partial x_j}\left[\left(\mu + \frac{\mu_t}{\sigma_\varepsilon}\right)\frac{\partial \varepsilon}{\partial x_j}\right] + C_{1\varepsilon}\frac{\varepsilon}{k}(G_k + C_{3\varepsilon}G_b) - C_{2\varepsilon}\rho\frac{\varepsilon^2}{k} + S_\varepsilon$$

In these equations, G_k represents the generation of turbulence kinetic energy due to the mean velocity gradients. G_b is the generation of turbulence kinetic energy due to buoyancy. Y_M represents the contribution of the fluctuating dilatation in compressible turbulence to the overall dissipation rate. $C_{1\varepsilon} = 1.44$ and $C_{2\varepsilon} = 1.92$ are constants, $\sigma_k = 1.0\ and\ \sigma_\varepsilon = 1.3$ are the turbulent Prandtl numbers for k and ε. S_k and S_ε are defined source terms.

The turbulent viscosity(μ_t), is obtained by k and ε,

$$\mu_t = \rho C_\mu \frac{k^2}{\varepsilon}$$

$C_\mu = 0.09$ is a constant.

2.3.7. The Volume Fraction Equation. The key of researching bubble behavior is an accurate description of movement of the bubbly two-phase fluid. The volume of fraction (VOF) model, which was put forward in 1981 by Hirt and Nichols, is a tracing inter-phase boundary method. It helps a lot solving volume fraction continuity equation on a fixed surface of one phase or several phases. [8]

Volume fraction equation for q^{th} phases was obtained to:

$$\frac{1}{\rho_q}\left[\frac{\partial}{\partial t}(\alpha_q\rho_q) + \nabla\cdot(\alpha_q\rho_q\overrightarrow{v_q}) = S_{\alpha_q} + \sum_{p=1}^{q}(\dot{m_{pq}} - \dot{m}_{qp})\right]$$

$\dot{m}_{qp}$ is the mass transfer from phase q to phase p and $\dot{m}_{pq}$ is the mass transfer from phase p to phase q.

Primary phase volume fraction calculation is based on below equation.

$$\sum_{q=1}^{n} \alpha_q = 1$$

The volume fraction equation may be solved either through implicit or explicit time discretization. When the implicit scheme for volume of fluid model is used for time discretization, ANSYS FLUENT's standard finite-difference interpolation schemes, QUICK, Second order upwind and first order upwind, and modified HRIC schemes, are used to obtain the face fluxes for all cells, including those near the interface. Time-dependent and steady-state calculations, both of them could use the implicit scheme to calculate.

In the explicit approach, ANSYS FLUENT's standard finite-difference interpolation schemes are applied to the volume fraction values that were computed at the previous time step. The face fluxes can be interpolated either using interface reconstruction or using a finite volume discretization scheme, when using the explicit scheme.

2.4. GAS-LIQUID FLOW

A mixture of phases means a large number of flows encountered in nature and technology. Physical phases of matter are gas, liquid, and solid, but the concept of phase in a multiphase flow system is applied in a broader sense. In multiphase flow, a phase can be defined as an identifiable class of material that has a particular inertial response to and interaction with the flow and the potential field in which it is immersed.

For multiphase flows, Fluent solves transport equations for two types of scalar: per phase and mixture. For an arbitrary k scalar in phase-I, FLUENT solves the transport equation inside the volume occupied by phase-I, denoted by $\emptyset_l^k$.

$$\frac{\partial \alpha_l \rho_l \emptyset_l^k}{\partial t} + \nabla \cdot \left(\alpha_1 \rho_1 \overrightarrow{u_l} \emptyset_l^k - \alpha_l \Gamma_l^k \nabla \emptyset_l^k\right) = S_l^k \quad k=1\ldots.. N$$

Where α_1, ρ_1, $\overrightarrow{u_l}$ are the volume fraction, physical density, and velocity of phase-I, respectively, Γ_l^k and S_l^k are the diffusion coefficient and source term.

In this case, scalar $\emptyset_l^k$ is associated only with one phase (phase-I), and is considered an individual field variable of phase-I.

When solving any multiphase problem, the first step is to determine which of the multiphase models best represents the flow. Advances in computational fluid mechanics have provided the basis for further insight into the dynamics of multiphase flow. Currently two approaches are used for the numerical calculation of multiphase flows: the Eular-Lagrange approach which treated the fluid as a continuum by solving the Navier-Stokes equations and the Euler-Euler approach- the different phases are treated mathematically as interpenetrating continua. In the Euler-Euler approach, it introduce a new concept that phasic volume by the volume of a phase cannot be occupied by the other phases, then these volume fractions are considered as continuous functions of space and time and the sum of all phases volume fraction is equal to 1. For general multiphase models, Fluent has three models from the Euler-Euler approach: volume of fluid (VOF) Model, Mixture Model, and Eulerian Model.

The volume of fluid (VOF) Model theory: Stratified flows, free-surface flows, filling sloshing, the motion of large bubbles in a liquid, the motion of liquid after a dam break, the prediction of jet breakup (surface tension), and the steady or transient tracking

of any liquid-gas interface are all included in the VOF model applications. A surface-tracking technique which is designed for two or more immiscible fluid where the position of the interface between the fluids is of interest applied to a fixed Eulerian mesh. In the VOF model, all fluids in the model shared a single set of momentum equations, and the volume fraction of each of the fluids in each computational cell is tracked throughout the domain.

The Mixture Model theory: It deals with some two or more phases (fluid or particulate) conditions included particle-laden flows with low loading, bubbly flows, sedimentation, and cyclone separators, and it also used for the dispersed phases to model homogeneous multiphase flow without relative velocities. Sine in the Eulerian model, the phases are treated as interpenetrating continua, the mixture model solves for the mixture momentum equation and prescribes relative velocities to describe the dispersed phases.

The Eulerian Model theory: this is the most complex of the multiphase models in Fluent. It was designed for the model of multiple separate, yet interacting phases (liquids, gases, or solids in nearly any combination) as bubble columns, risers, particle suspension, and fluidized beds. The Eulerian model solves a set of n momentum and continuity equations for each phase. Coupling is achieved through the pressure and interphase exchange coefficients. The manner in which this coupling is handled depends upon the type of phases involved; granular (fluid-solid) flows are handled differently than non-granular (fluid-fluid) flows. For granular flows, the properties are obtained from application of kinetic theory and momentum exchange between the phases.

2.5. PHYSICAL BOUNDARY CONDITIONS

The following list provides all boundary conditions could be used here in the Fluent. The inlet boundary conditions are determined by the situation at gas accumulation locations. Hydraulic input parameters for pumps determine the outlet boundary conditions.

There are five different inlet boundary conditions could be used in this ECCS piping. They are listed below:

- Mass-flow-inlet
- Velocity-inlet
- Inlet-vent
- Intake-fan
- Pressure-inlet

The allowable void volume calculation is based on the maximum system flow rate. Selection of maximum flow rates was the boundary condition setting here. The fluid which is water here is uncompressible, so velocity-inlet boundary condition is the only choice here.

Outlet boundary conditions could be used in this ECCS piping:

- Outflow
- Outlet-vent
- Pressure-outlet

Since the flow rate of the pump is the only parameter which could be used here, it couldn't define a boundary condition like outlet-vent and pressure-outlet conditions. So the outflow boundary condition satisfied this situation. The only parameter should be

defined for outflow boundary condition is the flow rate weighting, the portion of the outflow that is going through the boundary. The equation below is the calculation of the flow rate weighting.

$$\text{Flow Rate Weighting} = \frac{\text{Flow Rate Weighting specified on boundary}}{\text{Sum of all flow rate weightings}}$$

3. MODELS DESCRIPTION

3.1. OBJECTIVES

The objective of this thesis is to determine the maximum void that would enter the ECCS pump upon the intrusion of gas into the ECCS piping and ensure proper function of the ECCS as designed. The void entrainment transport in the ECCS was simulated using the ANSYS FLUENT 14.0 computational fluid dynamics package. The results from the simulation provided the basis data and images for the determination of the maximum allowable void. The maximum allowable void determined was compared with the result from "The gas transport testing conducted at Purdue University". A step-by-step approach is described for simulating the allowable initial gas volume at a piping system high-point based on allowable pump inlet void fractions:

Two models of typical ECCS piping which were based on Westinghouse Electric Company LLC project were developed by using ANSYS WORKBENCH 14.0 to simulate the void transport problem.

A significant assumption here is that the void is homogeneously distributed in the gas accumulation location. This assumption makes these 3D models possible since everything is uniform radially, thereby saving computational time.

The way of specification of the boundary conditions is to define the inlet boundary condition, the outlet boundary condition and assumption of the stable void transport time.

The inlet boundary condition was defined as the flow velocity condition at the gas accumulation location. The outlet boundary condition was defined as flow rate parameters at the pumps. Execution of the simulation for various void fractions at the

inlet until a stable time of transport is established. Stable void transport time, t_{stable} is defined as the time at which the void fraction at the pipe outlet (i.e. the pump inlet) becomes fairly constant with time.

The maximum allowable void fraction, α_{HP} at the inlet is defined by setting a limiting void fraction of 5% at the pump inlets. The limiting pump is the first pump to attain a void fraction of approximately 5% once a stable transport time is established.

This approach was adopted for two model problems as provided in the documentation of the simplified equation method. The simulation models for these problems are illustrated in next section. For the purpose of this simulation, we have defined a high-point at the elevation of the gas accumulation location. In both models, the gas accumulation locations are downstream of check valve along the emergency coolant supply lines.

3.2. MODEL 1

Model 1 shows a high point location downstream of the containment sump check valve. The high point location is outside of containment and could be monitored using ultrasonic transducers. During required post-accident operation, the high point pressure would be based on refueling water storage tank (RWST) head during normal operation and the pump pressure would be based on operation with sump in service.

The sump flow rate goes through the high point location and then travels down to the high pressure safety injection (HPSI) pump and single-stage (CS) pump. The layout for this problem is illustrated in Figure 3.1. The simulation model for this problem is illustrated in Figure 3.2.The data for the two pumps is shown in Table 3.1.

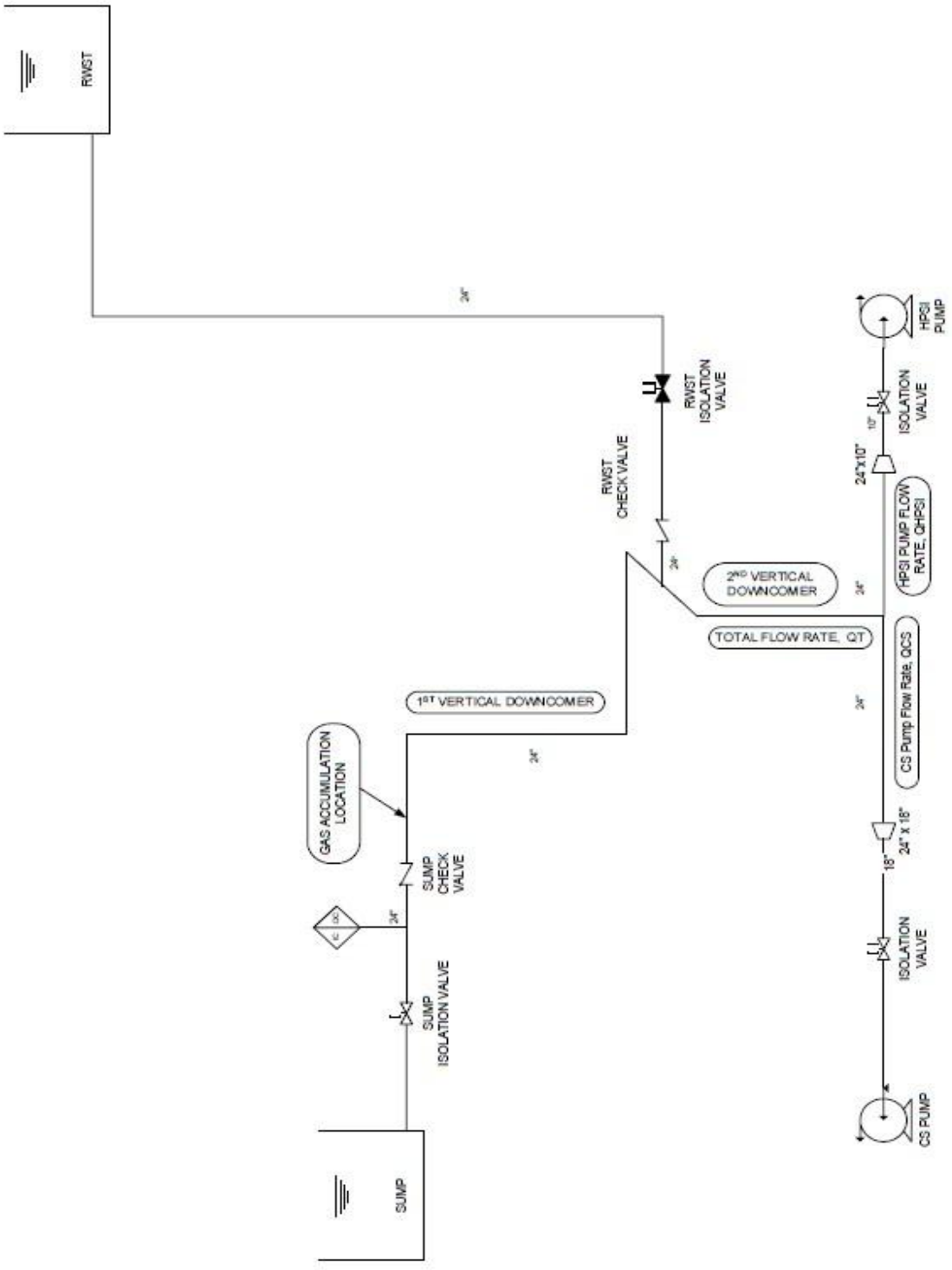

Figure 3.1: The Layout For Model 1

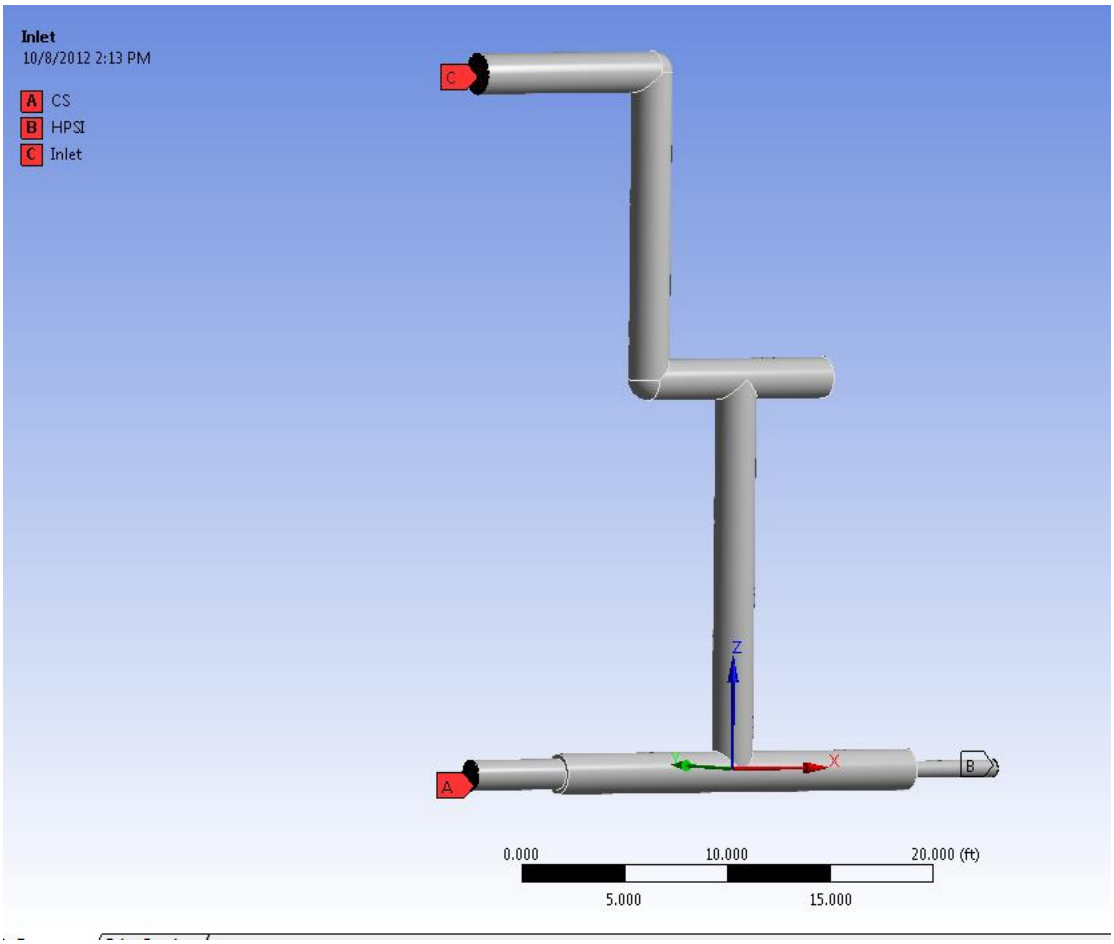

Figure 3.2: The Simulation Model Of Model 1

Table 3.1: The Pump Information Of Model 1

Pump Information		
Pump	HPSI	CS
Type	Muti-stage Stiff Shaft CA	Single-stage WDF
Best efficient point flow	900 gpm	4300 gpm
Maximum flow rate during post-accident recirculation mode of operation	1400 gpm	5200 gpm
Q/QBEP	1.56	1.21

Calculations of the velocity and pressure for each pump were listed below.

The maximum flow rate during post-accident recirculation mode of operation of CS pump:

$$Q_{CS} = \frac{5200\text{gal}}{\text{min}} = \frac{5200\text{gal}}{\text{min}} * \frac{1\text{ft}^3}{7.4805\text{gal}} * \frac{1\text{min}}{60\text{s}} \approx 11.5857\text{ft}^3/\text{s}$$

The area of the pipe at the entry into CS pump:

$$A_{CS} = \frac{\pi}{4}\left(\frac{D}{12}\right)^2 = \frac{3.1416}{4} * \left(\frac{18\text{in}}{\frac{12\text{in}}{\text{ft}}}\right)^2 \approx 1.7663\text{ft}^2$$

The maximum velocity during post-accident recirculation mode of operation of CS Pump:

$$v_{cs} = \frac{Q_{CS}}{A_{CS}} = \frac{11.5857\frac{\text{ft}^3}{\text{s}}}{1.7663\text{ft}^2} \approx 6.5593\ \text{ft/s}$$

The pressures at the entry into CS pump during post-accident recirculation mode of operation of CS pump:

$$P_{CS} = 25\text{psia} = 25\text{psia} * \frac{101325\text{Pa}}{14.7\text{psia}} \approx 172321.4286\text{Pa}$$

The flow rate weighing for CS pump during post-accident recirculation mode of operation of CS pump:

$$\beta = \frac{5200\text{gal/min}}{(5200 + 1400)\text{gal/min}} = 0.787879$$

The maximum flow rate during post-accident recirculation mode of operation of HPSI Pump:

$$Q_{HPSI} = \frac{1400\text{gal}}{\text{min}} = \frac{1400\text{gal}}{\text{min}} * \frac{1\text{ft}^3}{7.4805\text{gal}} * \frac{1\text{min}}{60\text{s}} \approx 2.6736\text{ft}^3/\text{s}$$

The area of the pipe at the entry into HPSI pump:

$$A_{HPSI} = \frac{\pi}{4}\left(\frac{D}{12}\right)^2 = \frac{3.1416}{4} * \left(\frac{10in}{\frac{12in}{ft}}\right)^2 \approx 0.5451ft^2$$

The maximum velocity during post-accident recirculation mode of operation of HPSI Pump:

$$v_{HPSI} = \frac{Q_{HPSI}}{A} = \frac{2.6736\frac{ft^3}{s}}{0.5451ft^2} \approx 4.9020\ ft/s$$

The pressure at HPSI pump suction pressure during post-accident recirculation mode of operation of HPSI pump:

$$P_{HPSI} = 26.3psia = 26.3psia * \frac{101325Pa}{14.7psia} \approx 181282.1429Pa$$

The flow rate weighing for HPSI pump during post-accident recirculation mode of operation of HPSI pump:

$$\beta = \frac{1400gal/min}{(5200 + 1400)gal/min} = 0.212121$$

The area of the pipe cross-section is:

$$A = \frac{\pi}{4}\left(\frac{D}{12}\right)^2 = \frac{3.1416}{4} * \left(\frac{23.25in}{\frac{12in}{ft}}\right)^2 \approx 2.9483ft^2$$

The maximum velocity during post-accident recirculation mode of operation at gas accumulation location:

$$v = \frac{Q_{HPSI} + Q_{CS}}{A} = \frac{\frac{(1400 + 5200)\ gal}{min} * \frac{1ft^3}{7.4805gal} * \frac{1min}{60s}}{2.9483} = 4.9876\ ft/s$$

The Flow rate weighting for CS and HPSI pump during post-accident recirculation mode of operation were calculated above. So flow rate weighting for CS and HPSI pump suction are 0.787879 and 0.212121. The velocity when fluid arrived before the pump CS, HPSI are 6.5594 ft/s, 5.72188 ft/s as showed at Table 3.2

Table 3.2: The Inlet And Outlet Boundary Condition Of Model 1

	Inlet	CS pump	HPSI pump
Velocity (ft/s)	4.9876	6.5594	5.72188
Flow rate weighting	1	0.787879	0.212121

3.3. MODEL 2

The intent of this Model 2 problem is to illustrate the overall methodology and demonstrate treatment of horizontal headers with off-takes. The layout for this problem is illustrated in Figure 3.3. The Figure shows a high point location downstream of the RWST check valve. The high point location is outside of containment and could be monitored using ultrasonic transducers. The sump flow rate goes through the high point location and then travels down to the low pressure safety injection (LPSI) pump, the high pressure safety injection (HPSI) pump and single-stage (CS) pump.

The simulation model for this problem is illustrated in Figure 3.4.

The layout for this problem is illustrated in Figure 3.3. The simulation model for this problem is illustrated in Figure 3.4. The data for those three pumps and the water entrance is shown in Table 3.3.

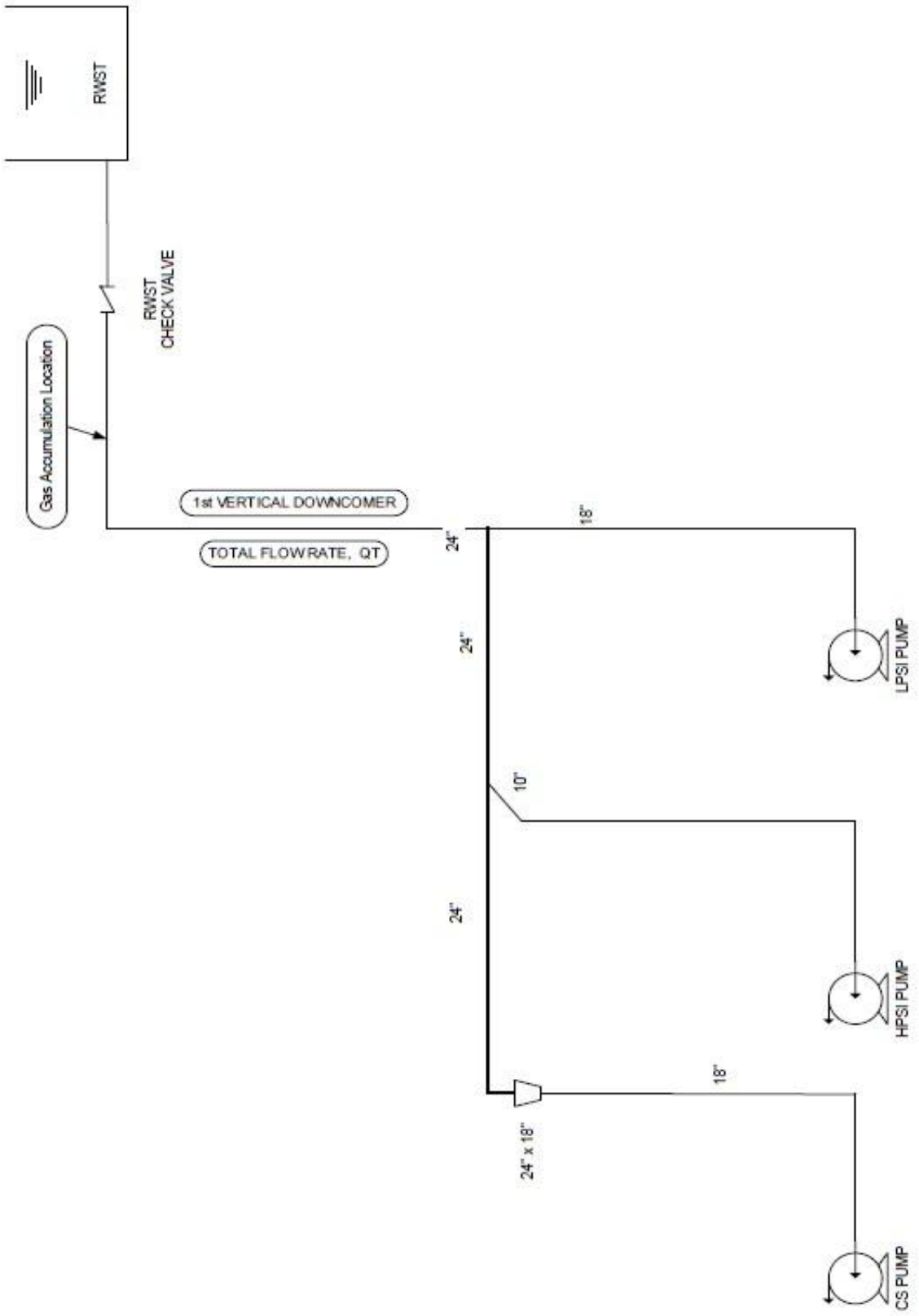

Figure 3.3: The Layout For Model 2

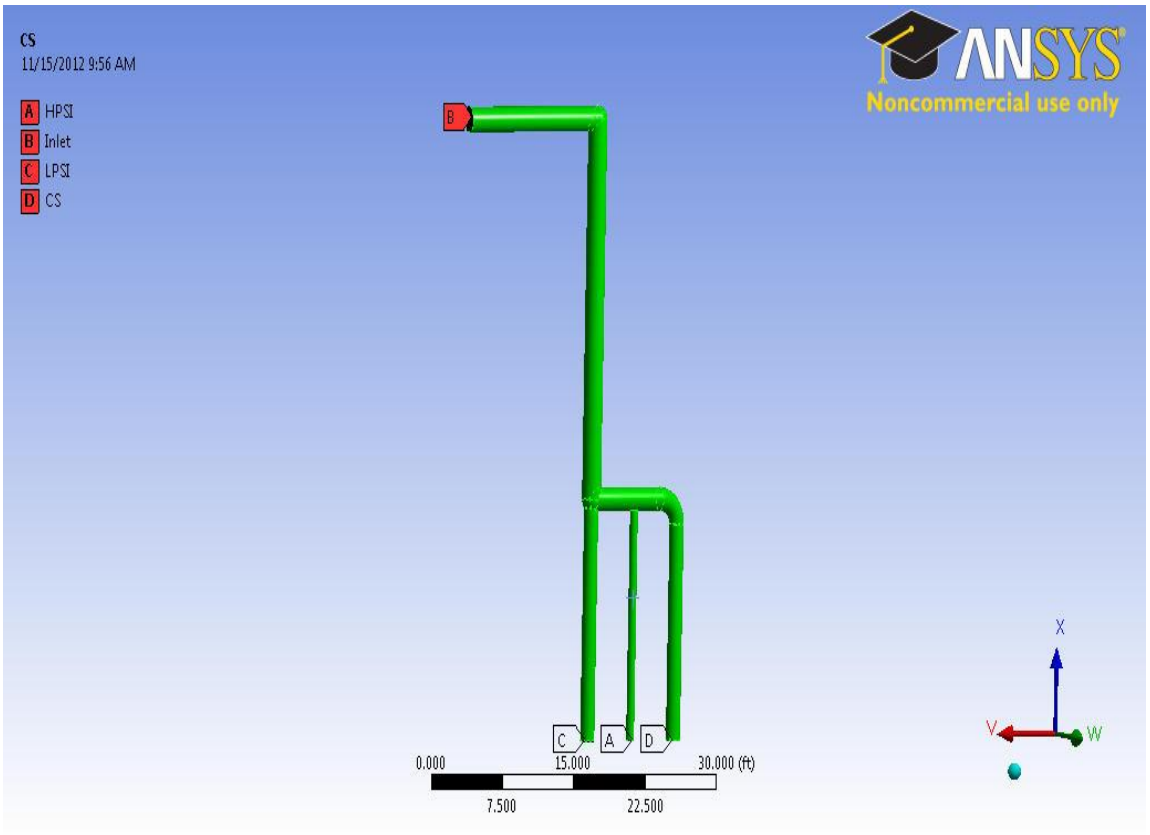

Figure 3.4: The Simulation Model Of Model 2

Table 3.3: The Pump Information Of Model 2

Pump Information			
Pump	HPSI	LPSI	CS
Type	Muti-stage Stiff Shaft	Single-stage	Single-stage
Best efficient point flow	900 gpm	4300 gpm	4300 gpm
Maximum flow rate during post-accident recirculation mode of operation	1400 gpm	5500 gpm	5200 gpm
Q/QBEP	1.56	1.28	1.21

Calculations of the velocity and pressure for each pump were listed below.

The area of the pipe cross-section:

$$A = \frac{\pi}{4}\left(\frac{D}{12}\right)^2 = \frac{3.1416}{4} * \left(\frac{23.25\text{in}}{\frac{12\text{in}}{\text{ft}}}\right)^2 \approx 2.9468\text{ft}^2$$

The maximum flow rate during post-accident recirculation mode of operation of CS pump:

$$Q_{CS} = \frac{5200\text{gal}}{\text{min}} = \frac{5200\text{gal}}{\text{min}} * \frac{1\text{ft}^3}{7.4805\text{gal}} * \frac{1\text{min}}{60\text{s}} \approx 11.5857\text{ft}^3/\text{s}$$

The area of the pipe at the entry into the CS pump:

$$A_{CS} = \frac{\pi}{4}\left(\frac{D}{12}\right)^2 = \frac{3.1416}{4} * \left(\frac{18\text{in}}{\frac{12\text{in}}{\text{ft}}}\right)^2 \approx 1.7663\text{ft}^2$$

The maximum velocity during post-accident recirculation mode of operation of CS pump:

$$v_{cs} = \frac{Q_{CS}}{A_{CS}} = \frac{11.5857\frac{\text{ft}^3}{\text{s}}}{1.7663\text{ft}^2} \approx 6.5593\ \text{ft/s}$$

The pressures at CS pump suction during post-accident recirculation mode of operation of CS Pump:

$$P_{CS} = 26.2\text{psia} = 26.2\text{psia} * \frac{101325\text{Pa}}{14.7\text{psia}} \approx 180592.857\text{Pa}$$

The flow rate weighing for CS pump during post-accident recirculation mode of operation of CS pump:

$$\beta = \frac{5200\text{gal/min}}{(5200 + +5500 + 1400)\text{gal/min}} = 0.429752$$

The maximum flow rate during post-accident recirculation mode of operation of HPSI pump:

$$Q_{HPSI} = \frac{1400gal}{min} = \frac{1400gal}{min} * \frac{1ft^3}{7.4805gal} * \frac{1min}{60s} \approx 3.1192ft^3/s$$

The area of the pipe at the entry into the HPSI pump:

$$A_{HPSI} = \frac{\pi}{4}\left(\frac{D}{12}\right)^2 = \frac{3.1416}{4} * \left(\frac{10in}{\frac{12in}{ft}}\right)^2 \approx 0.5451ft^2$$

The maximum velocity during post-accident recirculation mode of operation of HPSI pump:

$$v_{HPSI} = \frac{Q_{HPSI}}{A} = \frac{2.6736\frac{ft^3}{s}}{0.5451ft^2} \approx 5.7219\ ft/s$$

The pressure at HPSI pump suction pressure during post-accident recirculation mode of operation of HPSI pump:

$$P_{HPSI} = 26.9psia = 26.9psia * \frac{101325Pa}{14.7psia} \approx 185417.857Pa$$

The flow rate weighing for HPSI pump during post-accident recirculation mode of operation of HPSI pump:

$$\beta = \frac{1400gal/min}{(5200 + +5500 + 1400)gal/min} = 0.115702$$

The maximum flow rate during post-accident recirculation mode of operation of LPSI pump:

$$Q_{LPSI} = \frac{5500gal}{min} = \frac{5500gal}{min} * \frac{1ft^3}{7.4805gal} * \frac{1min}{60s} \approx 12.2541ft^3/s$$

The maximum velocity during post-accident recirculation mode of operation of LPSI pump:

$$v_{LPSI} = \frac{Q_{LPSI}}{A_{LPSI}} = \frac{12.2541 \frac{ft^3}{s}}{1.7663 ft^2} \approx 6.9379 ft/s$$

The pressure at LPSI pump suction pressure during post-accident recirculation mode of operation of LPSI pump:

$$P_{LPSI} = 25.8psia = 25.8psia * \frac{101325Pa}{14.7psia} \approx 177835.714Pa$$

The flow rate weighing for LPSI pump during post-accident recirculation mode of operation of LPSI pump:

$$\beta = \frac{5500gal/min}{(5200 + +5500 + 1400)gal/min} = 0.454545$$

The maximum velocity during post-accident recirculation mode of operation at gas accumulation location:

$$v = \frac{\frac{（1400 + 5200 + 5500）gal}{min} * \frac{1ft^3}{7.4805gal} * \frac{1min}{60s}}{2.9483} = 9.1485 ft/s$$

The pressure at CS, LPSI and HPSI pump suctions are the same with the pressure during post-accident recirculation mode of operation. Flow rate weighting for CS, LPSI and HPSI pump suction are 0.4298, 0.4545 and 0.1157. The velocity when fluid arrived before the pump CS, LPSI, and HPSI are 6.5594 ft/s, 6.9379 ft/s, 5.72188 ft/s which was presented at Table 3.4.

Table 3.4: The Inlet And Outlet Boundary Condition Of Model 2

	Inlet	CS pump	LPSI pump	HPSI pump
Velocity (ft/s)	9.1485	6.5594	6.9379	5.72188
Flow rate weighting	1	0.4298	0.4545	0.1157

4. METHOD OF SOLUTION

4.1. MESH GEOMETRY

This simulations were carried out as three dimensional transient flow pattern in models described below, using the commercial software FLUENT 14.0. At the gas accumulation location, water was considered as the continuous phase, and trapped gas was modeled as a sphere in the location. This was approximation was necessary because of the difficulty in modeling the accumulated gas in the realistic horizontal gas phase in the pipe section. To represent various trapped gas volumes, bubbles with radii 0.38 ft, 0.4 ft, 0.8 ft, 0.85 ft , and 0.9 ft were used in Model 1 and bubbles radii 0.60 ft, 0.65 ft, and 0.70 ft were used in the Model 2.

The structured grid within each block is generated using general curvilinear coordinates ensuring accurate representation of the flow boundaries. In order to select and adequate grid resolution, the effect of changing grid size was investigated.

For Model 1, the physical model and simulation model are presented shown in Figure 3.1 and Figure 3.2.

The meshing used was 0.002 ft as minimize size, 0.2 ft^2 as maximize face size, and 0.5 ft^3 as maximize volume size. Inflation was added at the inlet and outlet faces for the CS and HPSI pumps to enhance the element quality of the model. The total number of the elements is 233359, and 98280 is the nodes number. The average element quality is 0.6325. Note that for a good simulation, element quality should be less than 0.98. The lower the number, the better the simulation result and the longer it takes for the simulation to run.

For the model of Model 2, the physical model and the simulation model are presented in Figure 3.3 and Figure 3.4.

The meshing used was 0.0002 ft as minimize size, 0.02 ft^2 as maximize face size, and 0.0040 ft^3 as maximize volume size. Inflation was also added on the inlet and outlet faces of all pumps to enhance the element quality of the model. The total number of the elements is 543745, and 1694252 is the nodes number. The average element quality is 0.4982, less than 0.98.

Figure 4.1 is the mesh detail using layout method at the HPSI outlet, while Figure 4.2 is the mesh detail using layout method at the water inlet. The inflation parameters are identical for all faces on which one was defined.

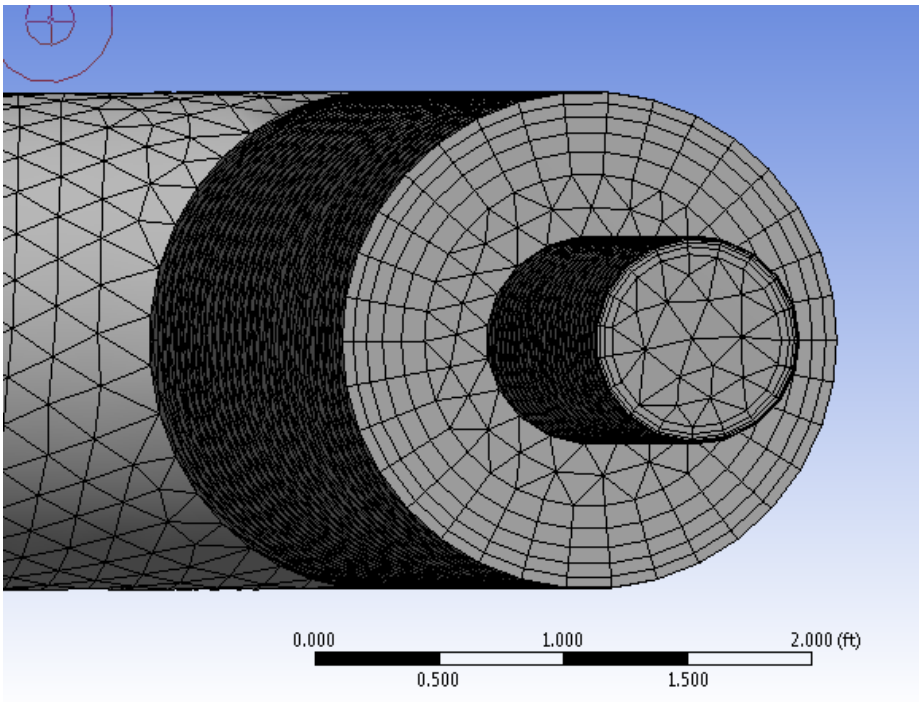

Figure 4.1: The Mesh Detail At The HPSI Outlet

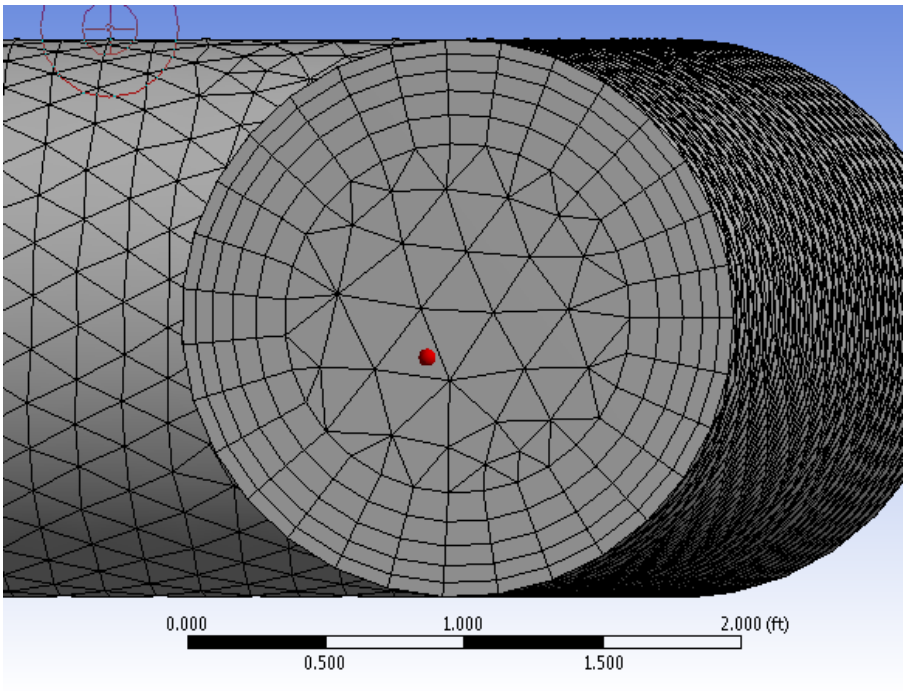

Figure 4.2: The Mesh Detail At The Water Inlet

4.2. INITIAL AND BOUNDARY CONDITIONS

The acceleration due to gravity was set at 32.19ft^2/s. The standard k-ε model was used. There was no heat-transfer was considered here in the model.

Since the simulation was for incompressible fluid with mechanical force motion, the inlet boundary conditions was set as the velocity boundary condition and outlet boundary conditions as outflow boundary condition.

For Model 1, the initial boundary condition is shown in Figure 4.3. It has a single bubble which is centered at the "x=-5, y=0, z=34" coordinate point. The boundary conditions of Model 1 are the inlet velocity is 4.9876 ft/s, flow rate weighting for CS and HPSI pump suction are 0.787879 and 0.212121.

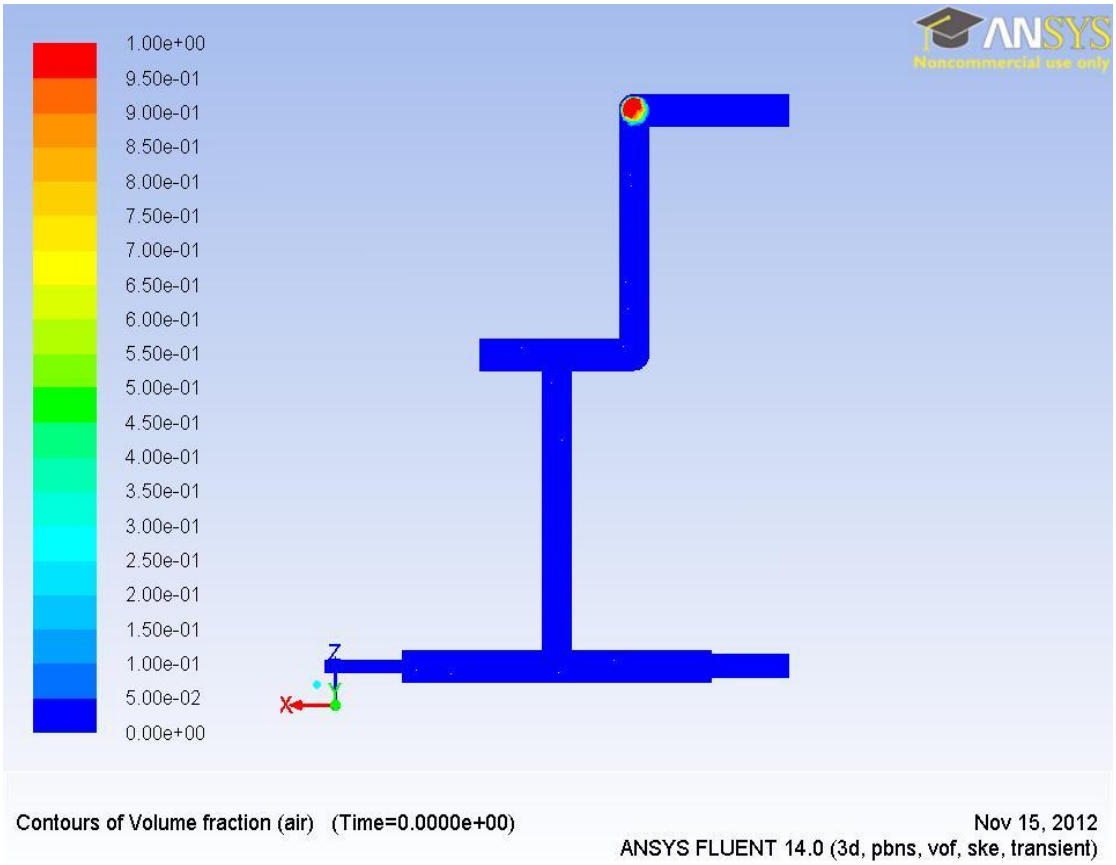

Figure 4.3: Initial Boundary Condition Of Model 1

For Model 2 , the initial boundary condition is shown in Figure 4.4. This has a single bubble which is centered at the position of "x=0.5, y=0, z=49". The inlet velocity was to 8.9927 ft/s, flow rate weighting for CS, LPSI and HPSI pump suction are 0.4298, 0.4545 and 0.1157

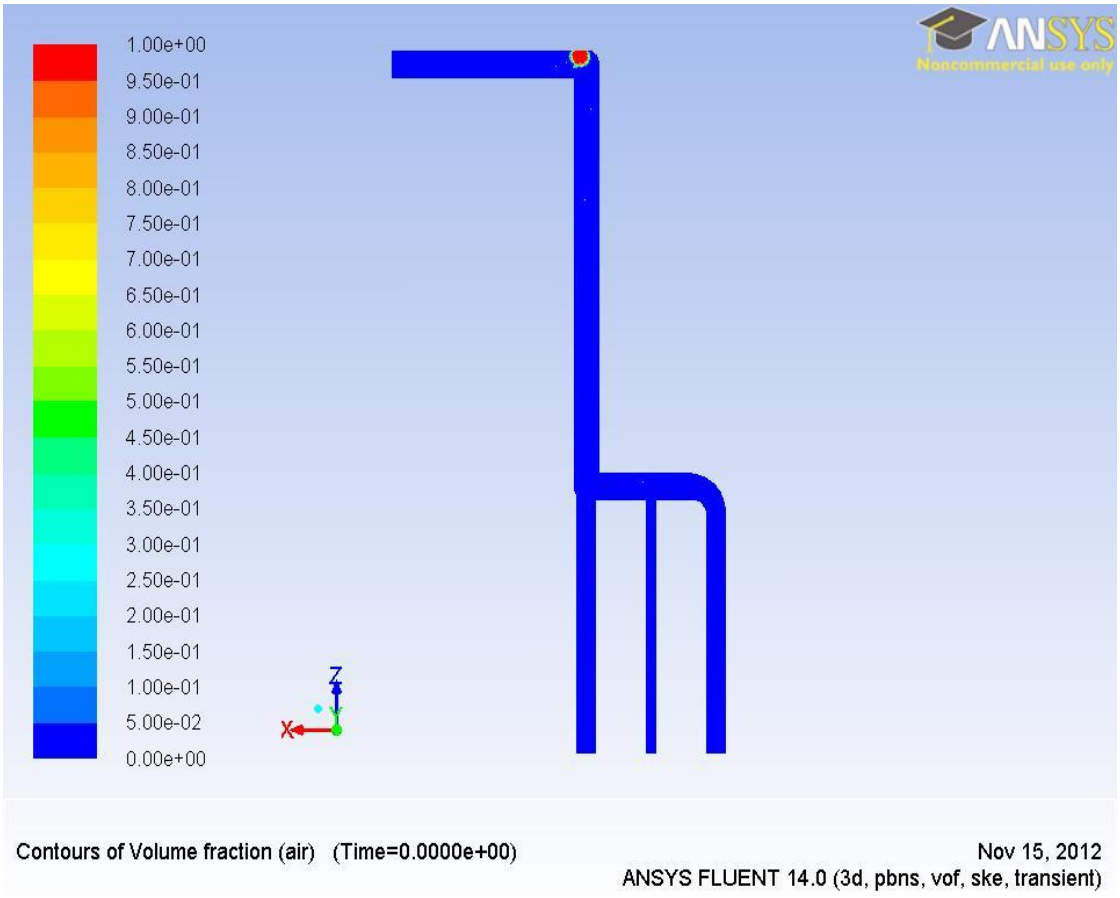

Figure 4.4: Initial Boundary Condition Of Model 2

5. RESULTS AND DISCUSSION

5.1. GAS VOLUME FRACTION PROFILES

At different time, the distributions of volume fraction at the CS pump outlet in Model 1 are not the same. Facet average volume fraction continued to increase after 25s, and peaked at 28s. Figures 5.1 to 5.8 show the transition in the bubble behavior at the CS pump outlet in Model 1.

Considering the gas volume fraction profiles below, gas gathered at the bottom of the pipe under the impaction of the fluid, subsequently, gases tended to accumulate at the top in piping system due by buoyancy. Before the simulation running for 28 seconds, the inertia force was the main force leading the gas went to the fluid moving direction. After 28 seconds, inertia force affected to the gas became smaller and smaller. The buoyancy would lead the gas go to the upside direction.

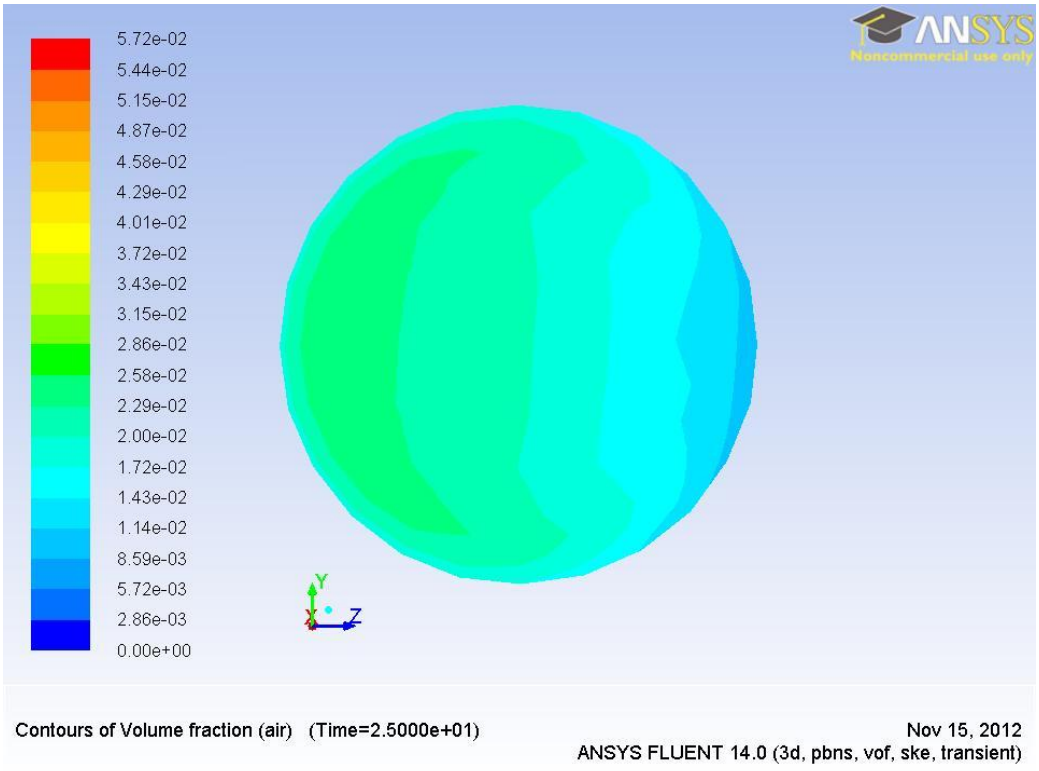

Figure 5.1: Contours Of Volume Fraction At T=25s

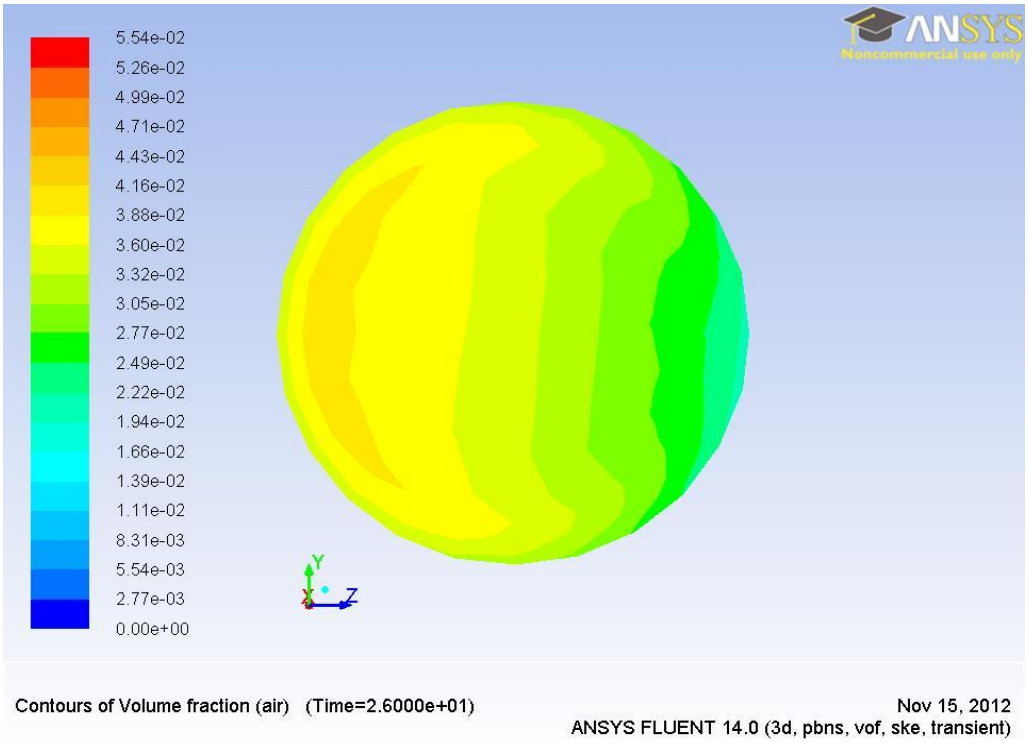

Figure 5.2: Contours Of Volume Fraction At T=26s

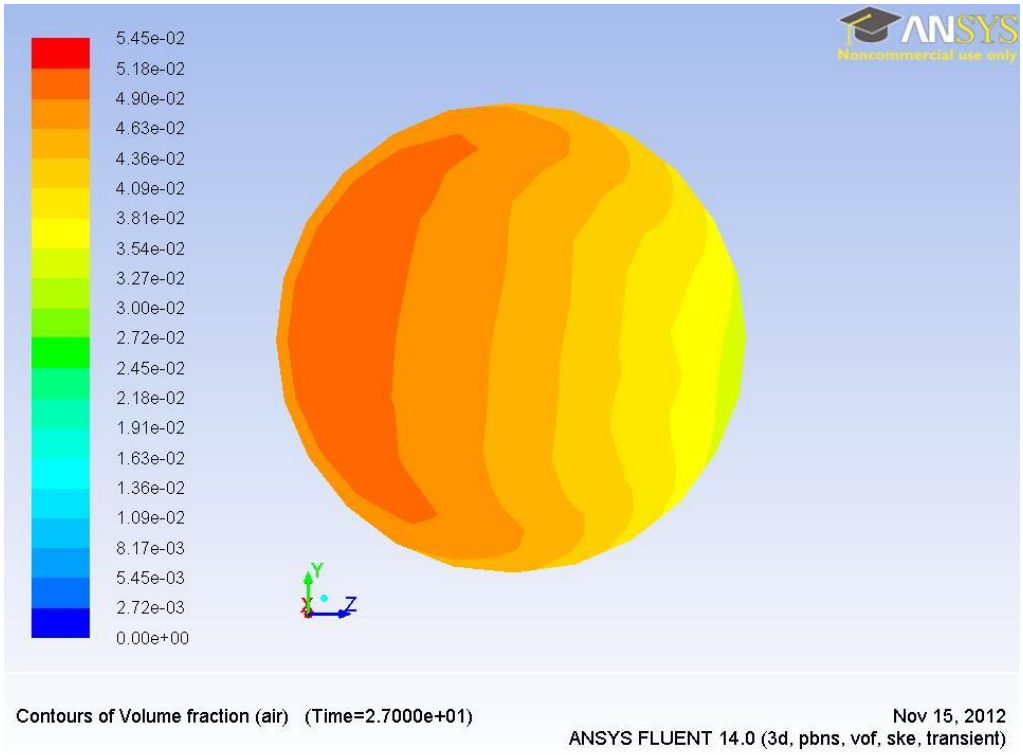

Figure 5.3: Contours Of Volume Fraction At T=27s

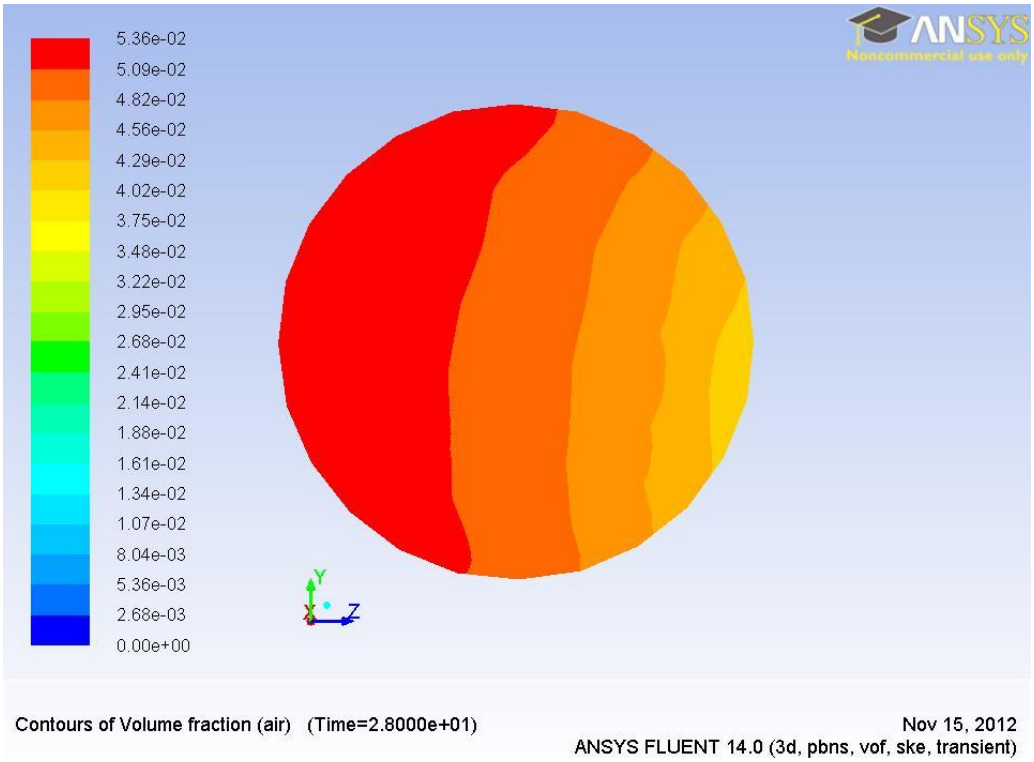

Figure 5.4: Contours Of Volume Fraction At T=28s

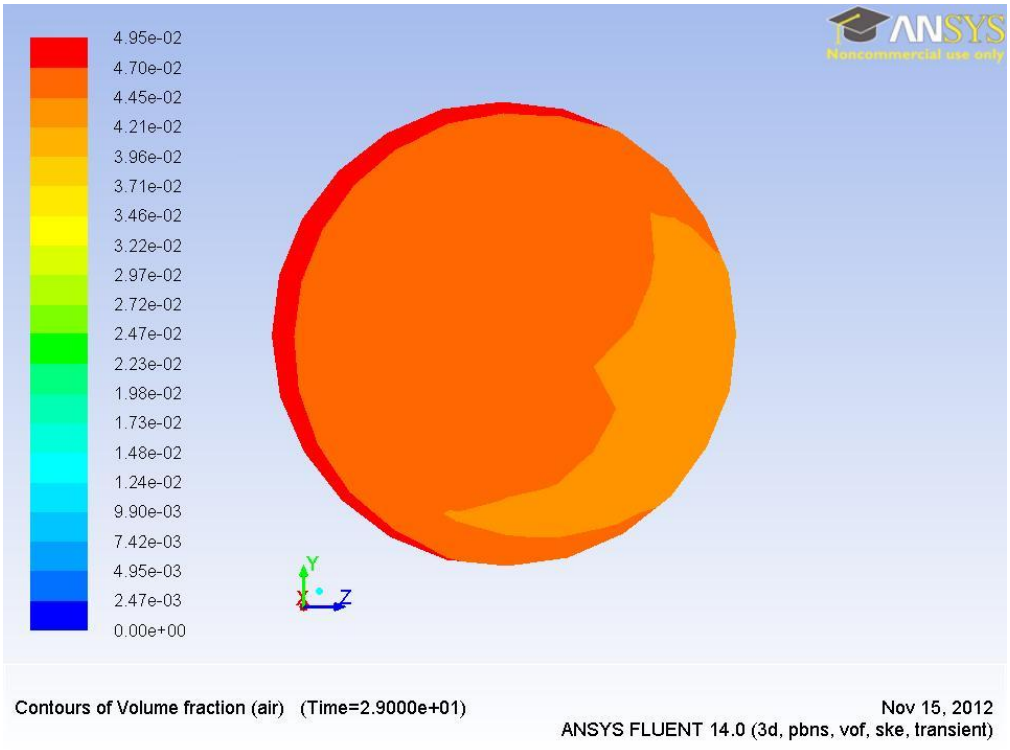

Figure 5.5: Contours Of Volume Fraction At T=29s

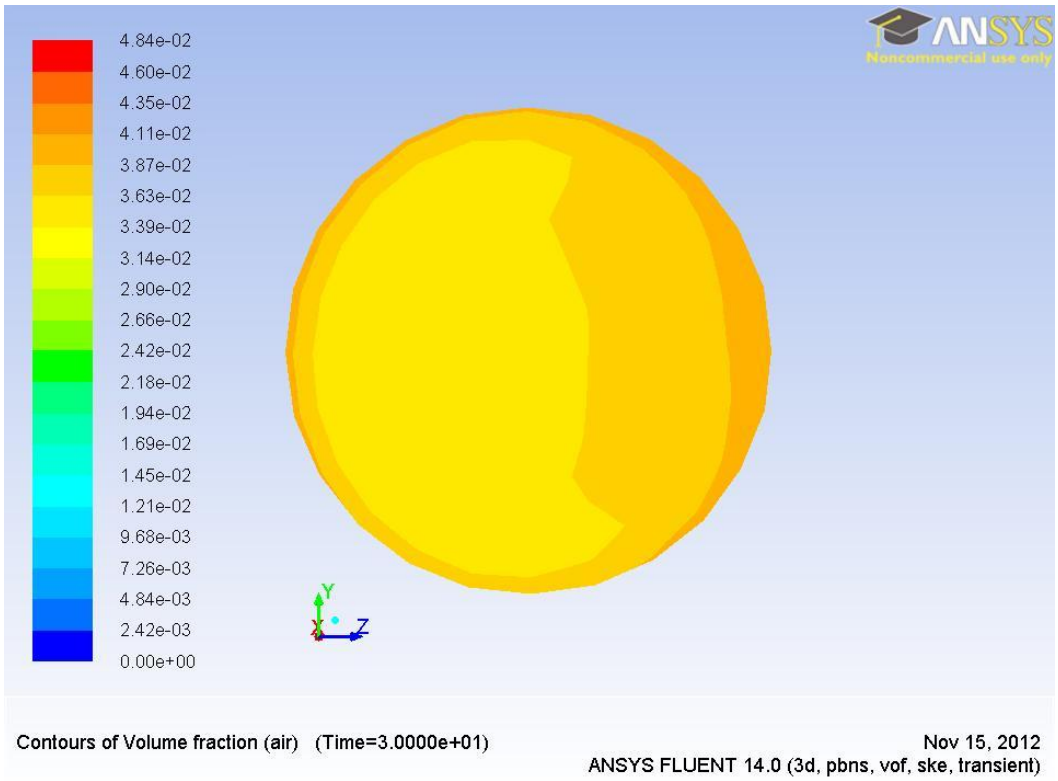

Figure 5.6: Contours Of Volume Fraction At T=30s

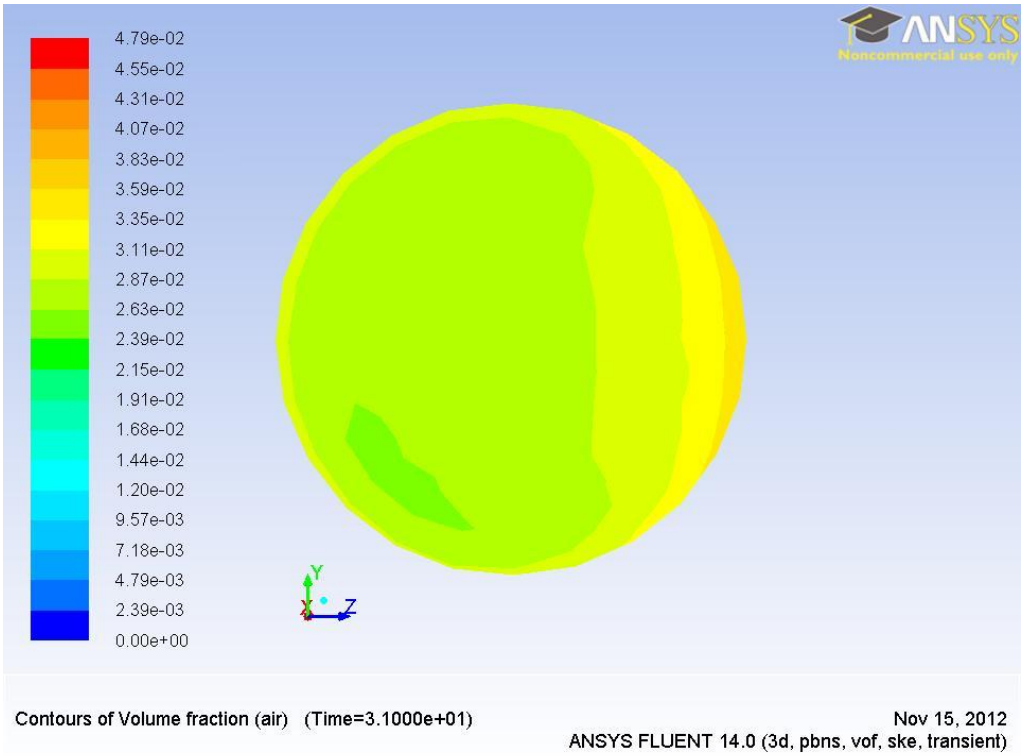

Figure 5.7: Contours Of Volume Fraction At T=31s

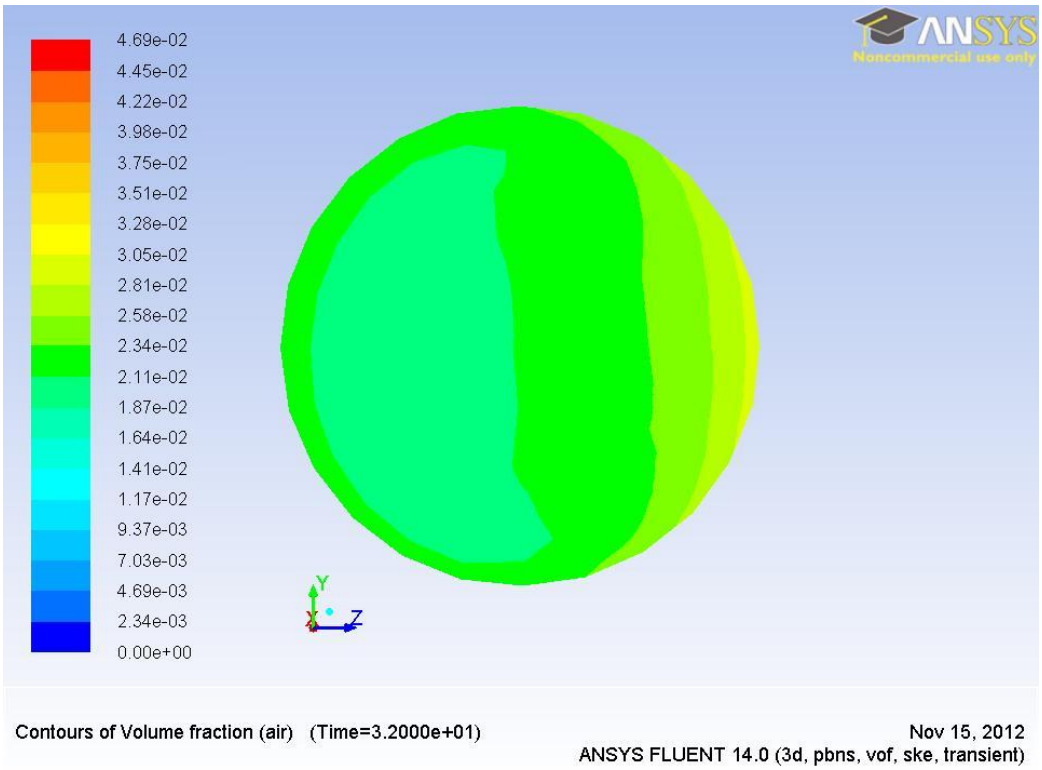

Figure 5.8: Contours Of Volume Fraction At T=32s

5.2. BUBBLE MEAN RADIUS

Various accumulated gas volumes were simulated in the Model 1 system using different gas bubble radius. The pumps with the limiting void fraction are the CS and HPSI in Model 1 and Model 2, respectively. Analysis of the void fraction entering the CS pump inlet for different radius – 0.38 ft, 0.4 ft, 0.8 ft, 0.85 ft , and 0.9 ft, – is shown in Figure 5.9. Also, Figure 5.10 represents the void fraction at the inlet to the HPSI pump different radius ranging from 0.6ft, 0.65ft to 0.70ft in Model 2.

5.3. THE MAXIMUM BUBBLE VOLUME IN THE ECCS AVOID DAMAGING THE PUMP

For Model 1, the bubble which radius is 0.8 ft is the biggest acceptable bubble size and after 28s, the number of volume fraction reached the peak. So the resultant gas volume allowed based on the simulation assumption is:

$$V_{allowable} = \frac{4}{3}\pi r^3 = \frac{4}{3}\pi(0.8)^3 = 2.1447\ ft^3$$

For Model 2, the bubble which radius is 0.65 ft is the biggest acceptable bubble size and at 12s, the number of volume fraction reached the peak. So the resultant gas volume allowed based on the simulation assumption is:

$$V_{allowable} = \frac{4}{3}\pi r^3 = \frac{4}{3}\pi(0.65)^3 = 1.1503\ ft^3$$

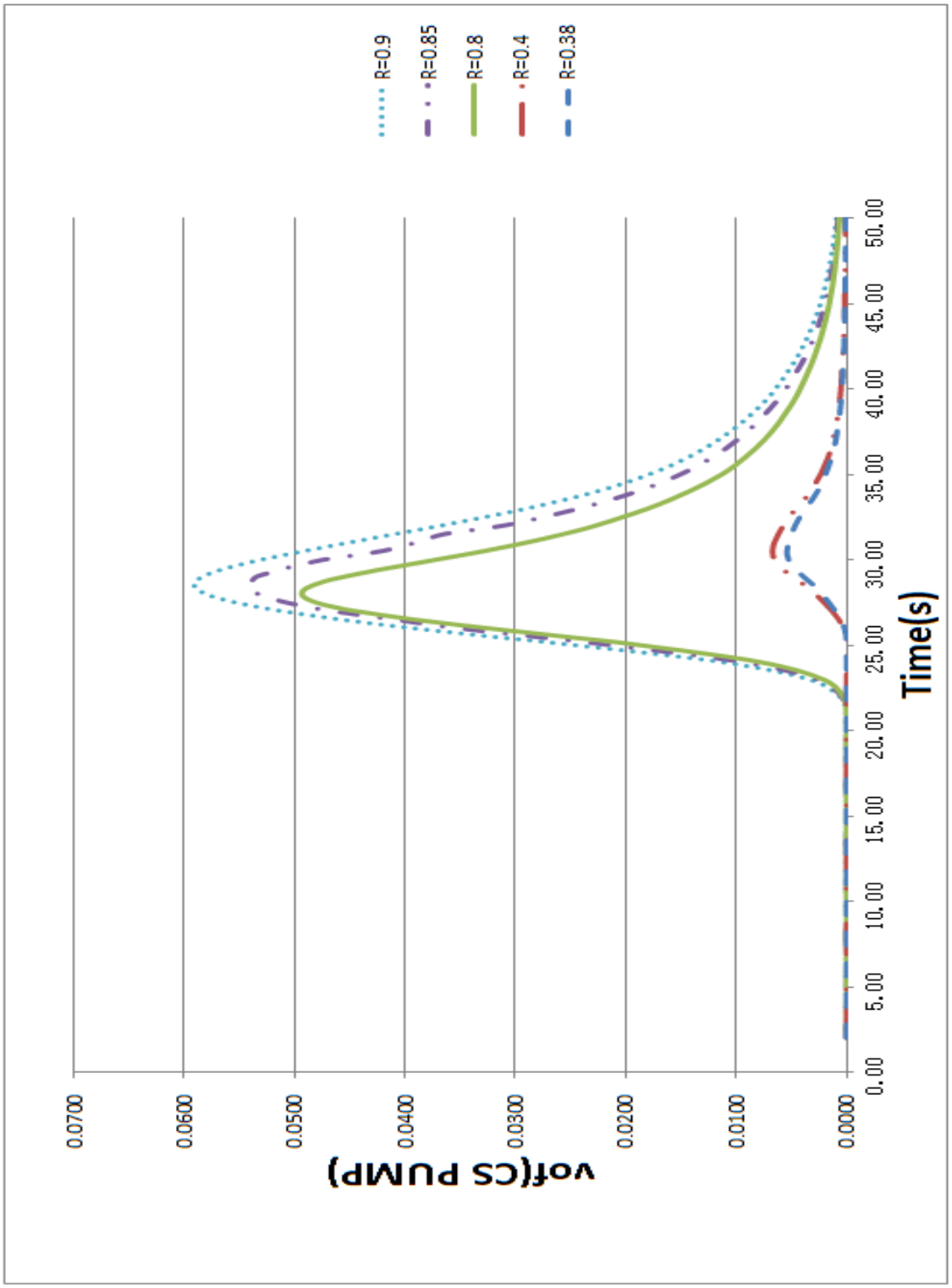

Figure 5.9 The Value Of Volume Fraction For Different Bubble Radius In Model 1

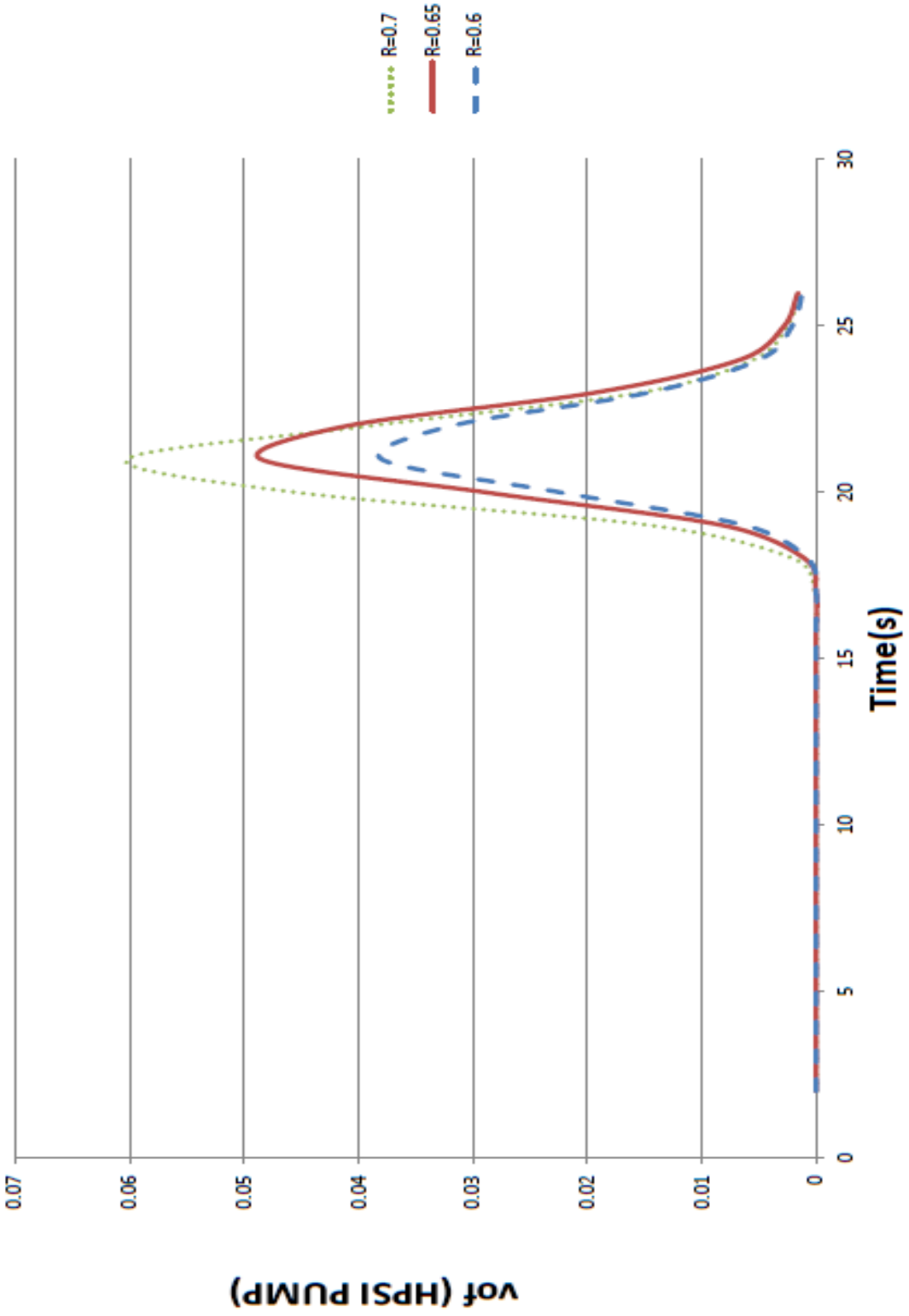

Figure 5.10 The Value Of Volume Fraction For Different Bubble Radius In Model 2

6. CONCLUSIONS AND FUTURE WORK

6.1. CONCLUSIONS

The analysis of the void introduction in the ECCS system is summarized as follows:

- The numerical values of void fraction at different outlets have been compared under different boundary conditions. The void fraction at the pump entry is affected by:
  - Void volume of gas accumulation location: the greater the gas at volume at the accumulation location, the higher the peak void fraction attainable at the pump inlets.
  - Layout of the piping: On different piping system, the value of void fraction at suction of the pump varies even when the same type of pump is used on different piping system.
- The void fractions at suction of the pumps are affected by other parameters such as the pump flow rate, pressure at the pump inlet and the elevation of the piping system to name a few.
- The allowable void at the accumulation point in each models are: 2.1447 ft^3 for Model 1 and 1.1503 ft^3 for Model 2.
  - The times at which the limitation void fractions were reached at the pump entry are 28 and 22 seconds for Models 1 and 2, respectively.

6.2. FUTURE WORK

Suggested future works in this project are:

- Simulation of more ECCS layout models
  - Two models were not enough to completely characterize the flow profile in this project. So a future task should be the simulation of more existing ECCS systems and development of models of typical ECCS piping.
- Mathematical model representing a first principle approach to evaluate allowable void in ECCS
  - A first principle approach to represent the mathematical model of the evaluating allowable void in ECCS is desirable. While simulations provide reliable results in this type of analysis, the drawback is the time it takes for the simulation to run. A decent CFD simulation of ECCS could run for several hours. If a mathematical model is developed, this will make the evaluation of allowable void faster and reliable.

BIBLIOGRAPHY

[1] Tariq Mahmood, "*Engineered safety feature, an emergency core cooling system at Pakistan research reactor-1*," (2007)

[2] United States Nuclear Regulatory Commission, "*50.46 Acceptance criteria for emergency core cooling systems for light-water nuclear power reactors*," http://www.nrc.gov/reading-rm/doc-collections/cfr/part050/part050-0046.html, (2012)

[3] Bal. Raj. Sehgal, "*Nuclear Safety in light water reactors*," Severe Accident Phenomenology, Light Water Reactor Safety, pp. 1-82, (2012)

[4] Zhang Yujie,LiuMingyan n, XuYonggui,TangCan, "*Three-dimensional volume of fluid simulations on bubble formation and dynamics in bubble columns*," (2012)

[5] K. Ekambara, R.S. Sanders, K. Nandakumar, J.H. Masliyah, "*CFD simulation of bubbly two-phase flow in horizontal pipes*," (2008)

[6] Eckhard Krepper, Dirk Lucas, Horst-Michael Prasser, "*On the modeling of bubbly flow in vertical pipes*"

[7] K. Ekambara, R.S. Sanders, K. Nandakumar*, J.H. Masliyah, "*CFD simulation of bubbly two-phase flow in horizontal pipes*,"(2007)

[8] John. D. Anderson, JR, "*Computational Fluid Dynamics*," The basics with applications, The Governing Equations of Fluid, pp. 60-93, (1995)

VITA

Lifeng Wang was born in Wuhan, China. In 2002, she graduated from The Second High School in Wuhan, China. Ms. Wang began her collegiate studies in 2005 and received a Bachelor of Science in Building Environment and Equipment Engineering in 2009 from Huazhong University of Science and Technology in Wuhan, China.

In August 2010, Ms. Wang joined the Missouri University of Science and Technology, Rolla, Missouri, in the Nuclear Engineering Program to earn her Master of Science degree, and she worked on an Ameren project regarding simulating the fluid fluent in the emergency core cooling system (ECCS) by utilizing ANSYS Fluent, in Missouri. She also worked as a Research Assistant on that project.